TITLE PAGE

Low-Grade Gliomas: Monitoring structural changes after chemotherapy using Diffusion Tensor MR Imaging-based Histogram Analysis and Functional Diffusion Maps

Antonella Castellano[1], MD, Marina Donativi[2], PhD, Roberta Rudà[3], MD,

Giorgio De Nunzio[2,4], PhD, Marco Riva[5], MD, Antonella Iadanza[1], MSc, Matteo Rucco[6], Msc,

Luca Bertero[3], MD, Lorenzo Bello[5], MD, Riccardo Soffietti[3], MD, and Andrea Falini[1], MD, PhD

1. Department of Neuroradiology and CERMAC, Università Vita-Salute San Raffaele and Ospedale San Raffaele, Milan, Italy

2. Department of Mathematics and Physics "Ennio De Giorgi" and A.D.A.M. (Advanced Data Analysis in Medicine), University of Salento, Lecce, Italy

3. Deparment of Neuro-oncology, University of Torino, Turin, Italy

4. INFN (National Institute of Nuclear Physics), Lecce, Italy

5. Department of Neurosurgery, University of Milano and Istituto Clinico Humanitas, Milan, Italy

6. School of Science and Technology, Computer Science Division, University of Camerino, Camerino (MC), Italy

Manuscript type: Original Research

Running title: Diffusion-Tensor MR Imaging in low-grade gliomas after chemotherapy

Corresponding author:

Antonella Castellano, MD

Neuroradiology Unit and CERMAC

Scientific Institute and Università Vita-Salute San Raffaele

Via Olgettina 60

20132 Milano

Italy

Phone: +39.02.2643.3015 - 3011

Fax: +39.02.2643.3447

Mail: castellano.antonella@hsr.it

Disclosure: Antonella Castellano conducted this study as partial fulfillment of her PhD in Molecular Medicine, Program in Experimental Neurology, San Raffaele University, Milan, Italy.

Conflict of interest: All the Authors are aware of the content of the paper and do not have any financial or other interests that might be construed as a conflict of interest.

Evaluation of low-grade gliomas structural changes after chemotherapy

using DTI-based histogram analysis and functional diffusion maps

Manuscript type: Original Article

Abstract

Objectives: To explore the role of diffusion tensor imaging (DTI)-based histogram analysis and functional diffusion maps (fDMs) in evaluating structural changes of low-grade gliomas (LGGs) receiving temozolomide (TMZ) chemotherapy.

Methods: Twenty-one LGG patients underwent 3T-MR examinations before and after three and six cycles of dose-dense TMZ, including 3D -fluid-attenuated inversion recovery (FLAIR) sequences and DTI (b=1000 s/mm^2, 32 directions). Mean diffusivity (MD), fractional anisotropy (FA), and tensor-decomposition DTI maps (p and q) were obtained. Histogram and fDM analyses were performed on coregistered baseline and post-chemotherapy maps. DTI changes were compared with modifications of tumor area and volume [according to Response Assessment in Neuro-Oncology (RANO) criteria], and seizure response.

Results: After three cycles of TMZ 20/21 patients were stable according to RANO criteria, but DTI changes were observed in all patients (Wilcoxon test, P≤.03). After 6 cycles, DTI changes were more pronounced (P≤.005). 75% of patients had early seizure response with significant improvement of DTI values, maintaining stability on FLAIR. Early changes of the 25th percentiles of p and MD predicted final volume change (R^2=.614 and .561, P<.0005, respectively). TMZ-related changes were located mainly at tumor borders on p and MD fDMs.

Conclusions: DTI-based histogram and fDM analyses are useful techniques to evaluate the early effects of TMZ chemotherapy in LGGs patients,.

Key words: Diffusion Tensor Imaging; Magnetic Resonance Imaging; glioma; chemotherapy; Response Evaluation Criteria

Key Points

1. DTI helps to assess the efficacy of chemotherapy in low-grade gliomas.

2. Histogram analysis on DTI metrics quantifies structural changes in tumor tissue.

3. Functional diffusion maps (fDMs) spatially localize the changes of DTI metrics.

4. Changes in DTI histograms and fDMs precede changes in conventional MRI.

5. Early changes in DTI histograms and fDMs correlate with seizure response.

Abbreviations and acronyms

DTI, diffusion tensor imaging

MRI, magnetic resonance imaging

fDM, functional diffusion maps

LGGs, low-grade gliomas

HGGs, high grade gliomas

WM, white matter

RANO, Response Assessment in Neuro-Oncology

FLAIR, fluid-attenuated inversion-recovery

TMZ, Temozolomide

PCV, Procarbazine, Lomustine and Vincristine

PR, partial response

mR, minor response

SD, stable disease

PD, progressive disease

vPR, volumetric partial response

vmR, volumetric minor response

vSD, volumetric stable disease

PD, volumetric progression of disease

ADC, apparent diffusion coefficient

FA, fractional anisotropy

MD, mean diffusivity

p, pure isotropic diffusion

q, pure anisotropic diffusion

IQR, interquartile range

ROC, receiver-operating characteristic

AUC, area under the ROC curve

Introduction

Low-grade gliomas (LGGs) are heterogeneous neoplasms with highly infiltrative behavior along white matter (WM) tracts [1]. These tumors are frequently located in or close to eloquent areas: tumor infiltration at functional subcortical borders reduces the chance to achieve a maximal surgical resection [2,3] and thus to impact prognosis [4-6]. Chemotherapy with PCV or TMZ represents an option in patients with incomplete resection, persisting seizures or progressive lesions on conventional MRI to avoid the risk of delayed neurotoxicity following radiotherapy [7-9]. Moreover, neoadjuvant TMZ chemotherapy may optimize the extent of surgical resection [10-12].

The assessment of response to chemotherapy in LGGs currently relies on Response Assessment in Neuro-Oncology (RANO) criteria [13] based on the evaluation of the cross-sectional area of T2/FLAIR abnormality, or on the tumor volumetry on T2/FLAIR images, which was found comparable [14] or superior [15,16] to linear diameters. However, these measurements are difficult in tumors with irregular shape and might not capture the real extent of infiltration beyond the borders of FLAIR abnormality. Moreover, following chemotherapy, a clinical improvement with

seizure reduction may not be predicted by tumor shrinkage on conventional MRI [17]. Thus, a better response assessment with advanced MRI techniques could improve patient management.

Diffusion-Tensor MR Imaging (DTI) is sensitive to the directional diffusion of water along WM tracts. A number of studies have attempted to use DTI to more precisely delineate the tumor margins and detect changes in the normal-appearing tissue surrounding malignant gliomas that are not evident on conventional MRI [18-20], with somewhat conflicting results [21]. In addition to mean diffusivity (MD) and fractional anisotropy (FA), some promising new metrics measuring the pure isotropic (p) and pure anisotropic (q) components of diffusion seem to be useful in depicting regions of infiltration surrounding the edge of the gross tumor [18,22,23], as confirmed by image-guided biopsies [24].

Recently, the changes in diffusion metrics of high grade gliomas (HGGs) following antiangiogenic therapy have been quantified over time by using histogram analysis on ADC maps [25,26]. Another approach to spatially localize the changes of diffusion parameters is based on the Functional Diffusion Maps (fDMs), which allow voxel-by-voxel comparison of measures over time with respect to a baseline map [27,28]. None of these DTI-based techniques has been used so far to evaluate the effects of chemotherapy in LGGs.

The aim of this study was to investigate whether DTI, as compared with standard MRI, could better detect microstructural tumor changes in patients with infiltrative LGGs receiving TMZ chemotherapy. More in detail, we evaluated the feasibility and reliability of histogram analysis and fDMs approaches on DTI maps to characterize and quantify the early effects of chemotherapy in LGGs.

Patients and methods

Twenty-one patients with histologically confirmed LGGs were retrospectively examined (15 men, 6 women; age, 34.5±7.7 years).

Demographic, clinical and histopathological data of patients are summarized in Table 1. At baseline, fourteen patients (67%) had seizures as a unique symptom.

The local ethical committee approved the study. Written informed consent for brain MRI was obtained from all patients.

MR Imaging

MRI was performed on a Philips Achieva 3.0T system (Best, the Netherlands).

Diffusion Tensor Imaging (DTI) data were obtained by a single-shot echo planar sequence with parallel imaging (SENSE factor R=2.5). Diffusion gradients were applied along 32 axes, using a b-value of 0 and 1000 s/mm^2. The detailed imaging parameters for DTI were: TR/TE, 8986/80; FOV, 24 cm; data matrix 96×96, interpolated in-plane to 256×256; section thickness, 2.5 mm; number of sections, 56; acquisition time, 5 minutes 23 seconds. The sequence was repeated two consecutive times and data were averaged off-line.

Conventional MRI sequences were: a) T2-weighted turbo spin-echo, b) T1-weighted inversion-recovery, c) three-dimensional fluid-attenuated inversion-recovery (3D-FLAIR) for tumor volumetry and d) post-gadolinium three-dimensional T1-weighted fast-field-echo (FFE). The detailed parameters for conventional MRI are provided in the Electronic Supplementary Materials.

Treatment and response assessment

MR studies were acquired at baseline and after 3 and 6 cycles of TMZ at a dose of 150 mg/m^2/die 1 week-on/1 week-off, without any concomitant treatment that could modify diffusion parameters (i.e. steroids). Patients who received chemotherapy had either persistent seizures with residual tumor after first surgery or a progressive tumor after initial watch and wait with MRI.

Response evaluation on MRI was performed *in consensus* by two board-certified neuroradiologists (*BLINDED*) and was based on measurement of both tumor area according to RANO criteria [13] and volume on 3D-FLAIR images [29]. Response cutoffs for volumetric measurements were derived from previous correlations of bidimensional measures with volume

[14,30]. Details on response criteria and the calculation of tumor volume are provided in the Electronic Supplementary Materials.

Seizure response was evaluated by two neuro-oncologists *in consensus* (*BLINDED*) according to standard criteria [13]: seizure reduction was significant when a ≥50% decrease in seizure frequency compared with baseline was observed, with concomitant anti-epileptic drugs being unchanged.

DTI data analyses

DTI data were analyzed using DTI Studio v2.4.01 software (H. Jiang, S. Mori, Johns Hopkins University, Baltimore), and diffusion tensor was calculated at each voxel, obtaining main eigenvector (λ_1, λ_2, λ_3), fractional anisotropy (FA) and Trace maps; from the elaboration of these datasets in Matlab 7.10.0 (The MathWorks, Natick, Massachusetts, 2010) mean diffusivity (MD) and tensor decomposition-derived pure isotropic (*p*) and pure anisotropic (*q*) maps were derived as follows [18]:

$$p = \sqrt{3}MD$$
$$q = \sqrt{(\lambda_1 - MD)^2 + (\lambda_2 - MD)^2 + (\lambda_3 - MD)^2}$$

At baseline, pathological areas were segmented on each map using a CAD (Computer-Aided Detection) system based on 3D Texture Analysis [31] giving automatically detected tumor regions-of-interest (ROIs). The ROIs were visually inspected and manually refined by a neuroradiologist (*BLINDED*).

The DTI studies acquired after 3 and 6 cycles of chemotherapy were aligned to baseline pretreatment scans with a linear registration algorithm (see details in Electronic Supplementary Material). Gray-level histograms and their main parameters (mean, median, 25th and 75th percentiles, interquartile range, skewness and kurtosis) were calculated at baseline in the ROIs, and compared to the values calculated in homologous contralateral regions. Histogram values within the tumor ROIs were also visualized by means of color overlays (see Electronic Supplementary

Material and Figure S1). Histogram parameters were then calculated within the same baseline tumor ROIs at follow-up, and their time evolution was assessed.

Functional Diffusion Map (fDM) analysis was performed according to [27,32]. Each post-treatment map was overlaid to the respective baseline map to compare voxel-by-voxel the same brain regions and to localize therapy-induced changes. Red or blue voxels indicated tumor regions with respectively a significant rise or decrease in DTI values compared to baseline (see Electronic Supplementary Material).

Statistical Analysis

Pairwise comparisons of histogram-derived parameters from p, q, MD and FA maps ROIs in tumor at baseline versus contralateral normal tissue and their changes after three and six cycles of treatment were assessed using the two-tailed Wilcoxon signed-rank test, with a significance level of $P<.05$.

Spearman's rank correlation was used to assess the relationship between percentage changes in histogram-derived DTI parameters and percentage change of tumor volume. Then, for each DTI map, a linear regression analysis was performed to determine the best predictor of final percentage of volume change after 6 cycles, considering the percentages of histogram-parameters changes after 3 cycles of TMZ as the independent variables. The parameters with high predictive power were selected to perform a binary logistic regression test and receiver-operating characteristic (ROC) curves were calculated to determine the diagnostic performance for early identifying responder or stable patients.

The Mann Whitney U test was used to evaluate the differences in percentages of changed voxels in fDMs according to clinical response.

Analysis and statistical figures were calculated with SPSS 20.0 (SPSS Inc., IBM, Chicago) and by in-house algorithms developed in Matlab.

Results

9

Patient and response assessment on MRI

Twenty-one patients were included: 16 had MR and DTI after 3 cycles of TMZ, while all 21 patients had both evaluations after 6 cycles.

At baseline, the median tumor area on FLAIR images was 19.43 cm^2 (range 2.15-73.15 cm^2); the median tumor volume on FLAIR images was 37.37 cm^3 (range 5.45-138.68 cm^2). No differences were found according to gender, histology and clinical presentation (Kruskal-Wallis test, $P \geq .05$).

Following 3 cycles of TMZ changes in tumor area were categorized as stable disease (SD) in 15/16 (93.7%) patients and progressive disease (PD) in 1/16 (6.2%). Changes in tumor volume were categorized as volumetric minor response (vmR) in 1/16 (6.2%) patients, volumetric stable disease (vSD) in 14/16 (87.5%) and volumetric progression of disease (vPD) in 1/16 (6.2%). Interestingly, in 11 out of 14 stable patients (78.5%) both according to RANO and volumetric criteria, a significant reduction of seizures was observed.

Following 6 cycles of TMZ changes in tumor area were categorized as partial response (PR) in 2/21 (9.5%), minor response (mR) in 5/21 (23.8%) patients, SD in 13/21 (61.9%) and PD in 1/21 (4.8%). Changes in tumor volume were categorized as vmR in 9/21 (42.8%) patients, vSD in 11/21 (52.4%) and vPD in 1/21 (4.8%).

DTI Histogram analysis

At baseline, DTI histograms showed significant differences between tumor ROIs and contralateral normal tissue (Table E1 online): changes were more significant on p, MD and FA rather than q maps. The volume of pathological hyperintense regions on p and MD maps was larger than the tumor volume on corresponding FLAIR images ($P<.001$). The distribution of histogram values within the tumor p region was visualized by color overlays (Figure S1 online): the median values of p were located within the center of the tumor, whereas the lower 25th percentile of p were located at the edge of the tumor; interestingly, the areas containing the voxels with values of p

below the 25th percentile extended beyond the edge of the FLAIR alteration, possibly representing regions of peritumoral infiltration.

Following chemotherapy, modifications of p, MD and FA values were seen in all patients (Table 2).

After 3 cycles of TMZ 15 patients displayed a SD according to RANO criteria (Figure 1) while pairwise comparisons demonstrated a significant reduction of 25th percentile values both in p histograms (P=.036) and MD histograms (P=.027) with an increase of skewness (P=.001) and kurtosis (P=.005) with respect to baseline maps. FA histograms showed an increase of interquartile range (IQR) (P=.003), mean and 75th percentiles values (P=.023), with a kurtosis reduction with respect to baseline (P=.006). Of particular interest was the significant, early reduction of median and 25th percentile of p and MD values (P=.018) and 75th percentile and IQR of FA values (P=.028 and .018, respectively) among those patients who had a significant decrease of seizure frequency.

After 6 cycles of TMZ in the same group of non-progressive patients all DTI changes were maintained and became more significant: there was a further reduction of 25th percentile values in p and MD histograms (P<.0005) with an increase of skewness (P<.0005) and kurtosis (P≤.003) with respect to baseline maps. On FA maps an increase of IQR, mean and 75th percentiles (P<.0005) values was confirmed, with a further reduction of kurtosis compared with baseline (P=.001).

Overall, these results suggest both an early tumor shrinkage at the tumor borders and a late reduction of the whole tumor volume.

In the progressive patient (Figure 2), changes were the opposite on each map: after 3 cycles of TMZ there was an increase of 25th percentile values on p (+10.6%) and MD histograms (+12%), with a reduction of skewness (p: -46.4%; MD: -38%), and a specular reduction of FA IQR (-24.7%), 75th percentile (-10.6%) and mean (-8.8%) values. After 6 cycles, a further increase of 25th percentile and median values on p histograms (+16.5% and +14.6%, respectively) as well as on MD histograms (+14.9% and +14.6%) was evident together with a further reduction of FA IQR (-35.9%), 75th percentile (-22.2%) and mean (-21.8%) values.

There were significant monotonic relationships between percentage changes of histogram parameters after 3 cycles of TMZ and final percentage changes of tumor volume following 6 cycles (Table E2, Electronic Supplementary Material). On p histograms, a linear regression established that the percentage change of 25th percentile values significantly predicted the final volume change, $F(1,15)=22.253$, $P<.0005$, $R^2=.614$. Similarly, on MD histograms the early percentage change of 25th percentile values significantly predicted the final volume change, $F(1,15)=17.899$, $P=.001$, $R^2=.561$.

The best early discriminant parameter of final volumetric tumor change was percentage change of 25th percentile values on p histograms (AUC=0.889; CI:0.623-0.990; $P<.0001$), whose reduction was significantly greater in patients with minor response than in stable patients (Figure 3, Table 3). Percentage change of 25th percentile on MD histograms had lower performance (AUC=0.806; CI:0.525-0.959; $P=.019$): the overall diagnostic performance of these markers was superior to the percentage change of FLAIR tumor volume after 3 cycles, that showed an AUC=0.778 (CI:0.519-0.957; $P=.022$) (Figure 3, Table 3).

Functional Diffusion Maps analysis

On fDM maps, changes of p, MD and FA values after chemotherapy were displayed as blue/red areas (voxels with significant value reduction/increase); changes were observed early during treatment at the tumor borders on p and MD and late in the whole tumor burden on FA fDMs (Figure 1 and 2).

Among patients with SD according to RANO criteria, after 3 cycles of TMZ, the median percentage of blue voxels with a reduction of p and MD values was 11.2% and 10.4%, respectively (Figure 1E), further increasing after 6 cycles (13.6% on p and 13.5% on MD) (Figure 1F). The median percentage of red voxels with increased FA was 2.1% after 3 cycles and 4.5% after 6 cycles of TMZ (Figure 1H e 1I). Interestingly, the median percentage of blue voxels on p and MD fDMs was higher in patients with seizure reduction ($P=.036$).

In the patient with PD, fDM analysis confirmed opposite changes on each map: after 3 cycles of TMZ the percentage of red voxels on p and MD fDMs was 31.3% and 27.8%, respectively (Figure 2E), and rose to 39.5% on p and 36.9% on MD fDMs after 6 cycles (Figure 2F); the percentage of blue voxels on FA fDMs was 3.5% after 3 cycles and 5.7% after 6 cycles (Figure 2H and 2I).

Discussion

This study suggests DTI-based histogram analysis as a reliable tool to detect and quantify early tissue changes, not apparent on conventional MRI, in LGGs following chemotherapy with temozolomide. It also demonstrates the feasibility of the fDM analysis of DTI maps for spatial localization of the changes of DTI metrics.

To our knowledge, this is the first study applying these techniques to evaluate the response of LGGs to chemotherapy. Radiological response assessment is challenging in these tumors, as the currently used RANO criteria, based on the measurement of tumor area [13], have low reliability in lesions with irregular shape or margins. Moreover, effective therapies reduce seizure frequency that often is not associated with tumor size reduction [11,17,33,34].

We found significant changes both in MD and FA and on pure isotropic (p) and pure anisotropic (q) maps. Some previous studies reported that p and q maps define different tumor regions [18,35]: the core showed reduced values of anisotropy and markedly increased isotropy, while the peripheral regions showed increased isotropy but normal anisotropy, correlating with tumour infiltration as confirmed by image-guided biopsies [24]. p is proportional to MD ($p=\sqrt{3}MD$), while q is a measure of the deviation of the eigenvalues from MD [22], thus the major difference between p/q and MD/FA metrics lies in the q/FA difference. Hence, we found similar results for p and MD maps. Interestingly, the volume of pathological regions on p and MD was larger than the volume on corresponding FLAIR images at baseline; thus, the difference between the two regions (p or MD ROI minus FLAIR ROI) could represent the peritumoral infiltration

undetectable on MRI. This border contained the 25th percentile of the p or MD distribution (Figure S1) within the tumor, in accordance with previous studies applying DTI-based histogram analysis in newly-diagnosed LGGs, which reported that the median values reflected the tumor core, while the edge contained the 25th percentile of diffusivity and the 75th percentile of FA values [36]. Conversely, it is very unlikely that the border beyond the FLAIR represents the peritumoral edema, that is not a common finding in LGGs given the slow growth rate and usually modest mass effect of these tumors. Furthermore, if this was the case the p and MD values within this border would be higher than the 75th percentile of the distribution. This is also in line with previous studies trying to differentiate edema and glioma infiltration by comparing the diffusivity values in the peritumoral regions of LGGs, HGGs and metastases [37-39].

The q metrics were less informative in characterizing LGGs, as significant q value changes were previously described only in the gross tumor core of HGGs [18,24].

The direction of changes of DTI parameters was related to patterns of water mobility in LGGs, where isotropic diffusion (p and MD) is higher than in normal tissue (Table 2 and E1). Indeed, in the early avascular, infiltrative stage of growth typical of LGGs, glioma cells remodel the extracellular matrix through secretion of matrix-degrading enzymes. This in turn leads to a widening of the extracellular space with an accumulation of water in large amounts [40]. This increased amount of extracellular water, along with a dense network of glioma cell processes that may hinder diffusion, are the dominant factors that lead to increased isotropy (p) and diffusivity (MD) and reduction of anisotropy in infiltrating LGGs. In line with these observations, the early effects of treatment consisted in a reduction of 25th percentile values of p and MD and an increase of skewness and kurtosis in the current study; changes in the domains of lower diffusivity (25th percentile), likely representing the regions of infiltrations, reflected an early tumor shrinkage in response to chemotherapy, which could occur from the infiltrative periphery to the lesion center. The parallel increase in skewness and kurtosis indicated that most of the values on isotropy maps histogram laid to the left of the mean and had a sharper peak compared with baseline; hence, a

general shift of MD and p histograms towards lower, 'normal' tissue diffusivity values may be the DTI 'signature' of chemotherapy response in LGGs. On FA maps, the increase of IQR and 75th percentile values indicated a general increase of anisotropy, reflecting a compaction of the whole tumor burden in response to treatment. Coherently, the opposite patterns were found in the patient with progressive disease.

Changes of DTI-histogram parameters showed strong correlations with volume changes, paralleling or even preceding tumor size reduction or increase on MRI. The best DTI parameter for an early identification of responders in the group of stable patients on conventional MRI was the percentage change of the 25th percentile on p, suggesting a potential value of this parameter as a biomarker for an early detection of chemotherapy activity. So far, an early detection of tumor response (especially after 3 months) does not impact treatment decisions, as the option to continue chemotherapy still relies on standard MRI criteria [13]; however, the proposed new method may represent a *proof of concept* that structural changes can occur very early during treatment. Hence in future trials early DTI changes could represent a biomarker of chemotherapy response and thus guide the duration of treatment.

Another novel result of this study is the demonstration of the feasibility, in DTI maps, of the fDM approach, indicating the areas of maximal tumor shrinkage at the periphery and guiding the decision of a second surgery to increase the extent of resection [10,12]. This clearly highlights the superiority of the DTI-based method with respect to a simple volumetric evaluation to accurately localize the sites of microstructural changes following chemotherapy. fDMs changes were prominent in patients who had a significant reduction of seizures: thus, DTI could detect minimal changes in tumor tissue of meaningful clinical significance, by predicting and visualizing patterns of LGGs shrinkage in response to chemotherapy. It is unlikely that this shrinkage reflects a decrease of surrounding edema, which in LGGs is generally absent. Furthermore, it is also unlikely that the changes in DTI parameters in LGGs after chemotherapy could be related to other phenomena such as a pseudoresponse or pseudoprogression, as they have been described only in HGGs following

either treatment with antiangiogenic agents or combined treatment with radiotherapy [41], and not in LGGs.

In the future, the use of more sophisticated analyses including Tract Based Spatial Statistics (TBSS) [37] may give further insights into the tumoral and peritumoral changes after treatments and the patterns of involvement of the surrounding WM structures.

This preliminary study has some limitations, such as the small number of patients in which DTI sequences were available at all time points and the short-term follow-up. All these data must be confirmed in larger prospective studies comparing patients with and without response to chemotherapy to define whether these advanced MRI techniques could also be useful to predict tumor progression in LGGs.

In conclusion, DTI-based histogram and fDM analyses are useful techniques to evaluate the early effects of TMZ chemotherapy in LGG, preceding modifications on conventional MRI and volumetry. fDM analysis is feasible on DTI maps in LGGs and allows to visualize the heterogeneity of treatment response within the same lesion, thus improving the evaluation of chemotherapy efficacy.

References

1. Rudà R, Trevisan E, Soffietti R (2012) Low-grade gliomas. Handb Clin Neurol 105:437-450. Doi:10.1016/B978-0-444-53502-3.00001-X

2. Castellano A, Bello L, Michelozzi C et al (2012) Role of diffusion tensor magnetic resonance tractography in predicting the extent of resection in glioma surgery. Neuro Oncol 14:192-202. Doi:10.1093/neuonc/nor188

3. Talos IF, Zou KH, Ohno-Machado L et al (2006) Supratentorial low-grade glioma resectability: Statistical predictive analysis based on anatomic MR features and tumor characteristics. Radiology 239:506-513. Doi:10.1148/radiol.2392050661

4. Smith JS, Chang EF, Lamborn KR et al (2008) Role of extent of resection in the long-term outcome of low-grade hemispheric gliomas. J Clin Oncol 26:1338-1345. Doi:10.1200/JCO.2007.13.9337

5. Soffietti R, Baumert BG, Bello L et al (2010) Guidelines on management of low-grade gliomas: Report of an EFNS-EANO task force. Eur J Neurol 17:1124-1133. Doi:10.1111/j.1468-1331.2010.03151.x

6. Keles GE, Lamborn KR, Berger MS (2001) Low-grade hemispheric gliomas in adults: A critical review of extent of resection as a factor influencing outcome. J Neurosurg 95:735-745

7. Brada M, Viviers L, Abson C et al (2003) Phase II study of primary temozolomide chemotherapy in patients with WHO grade II gliomas. Ann Oncol 14:1715-1721

8. Pace A, Vidiri A, Galie E et al (2003) Temozolomide chemotherapy for progressive low-grade glioma: Clinical benefits and radiological response. Ann Oncol 14:1722-1726

9. van den Bent MJ, Afra D, de Witte O et al (2005) Long-term efficacy of early versus delayed radiotherapy for low-grade astrocytoma and oligodendroglioma in adults: The EORTC 22845 randomised trial. Lancet 366:985-990. Doi:10.1016/S0140-6736(05)67070-5

10. Duffau H, Taillandier L, Capelle L (2006) Radical surgery after chemotherapy: A new therapeutic strategy to envision in grade II glioma. J Neurooncol 80:171-176. Doi:10.1007/s11060-006-9168-3

11. Blonski M, Taillandier L, Herbet G et al (2012) Combination of neoadjuvant chemotherapy followed by surgical resection as a new strategy for WHO grade II gliomas: A study of cognitive status and quality of life. J Neurooncol 106:353-366. Doi:10.1007/s11060-011-0670-x

12. Blonski M, Pallud J, Goze C et al (2013) Neoadjuvant chemotherapy may optimize the extent of resection of world health organization grade II gliomas: A case series of 17 patients. J Neurooncol 113:267-275. Doi:10.1007/s11060-013-1106-6

13. van den Bent MJ, Wefel JS, Schiff D et al (2011) Response assessment in neuro-oncology (a report of the RANO group): Assessment of outcome in trials of diffuse low-grade gliomas. Lancet Oncol 12:583-593. Doi:10.1016/S1470-2045(11)70057-2

14. Galanis E, Buckner JC, Maurer MJ et al (2006) Validation of neuroradiologic response assessment in gliomas: Measurement by RECIST, two-dimensional, computer-assisted tumor area, and computer-assisted tumor volume methods. Neuro Oncol 8:156-165. Doi:10.1215/15228517-2005-005

15. Sorensen AG, Patel S, Harmath C et al (2001) Comparison of diameter and perimeter methods for tumor volume calculation. J Clin Oncol 19:551-557

16. Dempsey MF, Condon BR, Hadley DM (2005) Measurement of tumor "size" in recurrent malignant glioma: 1D, 2D, or 3D? AJNR Am J Neuroradiol 26:770-776

17. Rudà R, Bello L, Duffau H, Soffietti R (2012) Seizures in low-grade gliomas: Natural history, pathogenesis, and outcome after treatments. Neuro Oncol 14 Suppl 4:iv55-64. Doi:10.1093/neuonc/nos199

18. Price SJ, Pena A, Burnet NG et al (2004) Tissue signature characterisation of diffusion tensor abnormalities in cerebral gliomas. Eur Radiol 14:1909-1917. Doi:10.1007/s00330-004-2381-6

19. Goebell E, Paustenbach S, Vaeterlein O et al (2006) Low-grade and anaplastic gliomas: Differences in architecture evaluated with diffusion-tensor MR imaging. Radiology 239:217-222. Doi:2383050059 [pii]; 10.1148/radiol.2383050059

20. Stadlbauer A, Nimsky C, Buslei R et al (2007) Diffusion tensor imaging and optimized fiber tracking in glioma patients: Histopathologic evaluation of tumor-invaded white matter structures. Neuroimage 34:949-956. Doi:S1053-8119(06)00875-5 [pii]; 10.1016/j.neuroimage.2006.08.051

21. Sternberg EJ, Lipton ML, Burns J (2014) Utility of diffusion tensor imaging in evaluation of the peritumoral region in patients with primary and metastatic brain tumors. AJNR Am J Neuroradiol 35:439-444. Doi:10.3174/ajnr.A3702

22. Pena A, Green HA, Carpenter TA, Price SJ, Pickard JD, Gillard JH (2006) Enhanced visualization and quantification of magnetic resonance diffusion tensor imaging using the p:Q tensor decomposition. Br J Radiol 79:101-109. Doi:10.1259/bjr/24908512

23. Price SJ, Jena R, Burnet NG, Carpenter TA, Pickard JD, Gillard JH (2007) Predicting patterns of glioma recurrence using diffusion tensor imaging. Eur Radiol 17:1675-1684. Doi:10.1007/s00330-006-0561-2

24. Price SJ, Jena R, Burnet NG et al (2006) Improved delineation of glioma margins and regions of infiltration with the use of diffusion tensor imaging: An image-guided biopsy study. AJNR Am J Neuroradiol 27:1969-1974

25. Nowosielski M, Recheis W, Goebel G et al (2011) ADC histograms predict response to anti-angiogenic therapy in patients with recurrent high-grade glioma. Neuroradiology 53:291-302. Doi:10.1007/s00234-010-0808-0

26. Pope WB, Qiao XJ, Kim HJ et al (2012) Apparent diffusion coefficient histogram analysis stratifies progression-free and overall survival in patients with recurrent GBM treated with bevacizumab: A multi-center study. J Neurooncol 108:491-498. Doi:10.1007/s11060-012-0847-y

27. Hamstra DA, Chenevert TL, Moffat BA et al (2005) Evaluation of the functional diffusion map as an early biomarker of time-to-progression and overall survival in high-grade glioma. Proc Natl Acad Sci U S A 102:16759-16764. Doi:10.1073/pnas.0508347102

28. Ellingson BM, Malkin MG, Rand SD et al (2010) Validation of functional diffusion maps (fDMs) as a biomarker for human glioma cellularity. J Magn Reson Imaging 31:538-548. Doi:10.1002/jmri.22068

29. Belhawi SM, Hoefnagels FW, Baaijen JC et al (2011) Early postoperative MRI overestimates residual tumour after resection of gliomas with no or minimal enhancement. Eur Radiol 21:1526-1534. Doi:10.1007/s00330-011-2081-y

30. Therasse P, Arbuck SG, Eisenhauer EA et al (2000) New guidelines to evaluate the response to treatment in solid tumors. european organization for research and treatment of cancer, national cancer institute of the united states, national cancer institute of canada. J Natl Cancer Inst 92:205-216

31. De Nunzio G, Pastore G, Donativi M, Castellano A, Falini A (2011) A CAD system for cerebral glioma based on texture features in DT-MR images. Nucl Instr and Meth A. Doi:10.1016/j.nima.2010.12.086

32. Moffat BA, Chenevert TL, Lawrence TS et al (2005) Functional diffusion map: A noninvasive MRI biomarker for early stratification of clinical brain tumor response. Proc Natl Acad Sci U S A 102:5524-5529. Doi:10.1073/pnas.0501532102

33. O'Connor JP, Jackson A, Asselin MC, Buckley DL, Parker GJ, Jayson GC (2008) Quantitative imaging biomarkers in the clinical development of targeted therapeutics: Current and future perspectives. Lancet Oncol 9:766-776. Doi:10.1016/S1470-2045(08)70196-7

34. Sherman JH, Moldovan K, Yeoh HK et al (2011) Impact of temozolomide chemotherapy on seizure frequency in patients with low-grade gliomas. J Neurosurg 114:1617-1621. Doi:10.3171/2010.12.JNS101602

35. Jones TL, Byrnes TJ, Yang G, Howe FA, Bell BA, Barrick TR (2014) Brain tumor classification using the diffusion tensor image segmentation (D-SEG) technique. Neuro Oncol. Doi:nou159 [pii]

36. Khayal IS, McKnight TR, McGue C et al (2009) Apparent diffusion coefficient and fractional anisotropy of newly diagnosed grade II gliomas. NMR Biomed 22:449-455. Doi:10.1002/nbm.1357

37. Hoefnagels FW, De Witt Hamer P, Sanz-Arigita E et al (2014) Differentiation of edema and glioma infiltration: Proposal of a DTI-based probability map. J Neurooncol 120:187-198. Doi:10.1007/s11060-014-1544-9

38. Pavlisa G, Rados M, Pavlisa G, Pavic L, Potocki K, Mayer D (2009) The differences of water diffusion between brain tissue infiltrated by tumor and peritumoral vasogenic edema. Clin Imaging 33:96-101. Doi:10.1016/j.clinimag.2008.06.035

39. Min ZG, Niu C, Rana N, Ji HM, Zhang M (2013) Differentiation of pure vasogenic edema and tumor-infiltrated edema in patients with peritumoral edema by analyzing the relationship of axial and radial diffusivities on 3.0T MRI. Clin Neurol Neurosurg 115:1366-1370. Doi:10.1016/j.clineuro.2012.12.031

40. Zamecnik J (2005) The extracellular space and matrix of gliomas. Acta Neuropathol 110:435-442. Doi:10.1007/s00401-005-1078-5

41. Wen PY, Macdonald DR, Reardon DA et al (2010) Updated response assessment criteria for high-grade gliomas: Response assessment in neuro-oncology working group. J Clin Oncol 28:1963-1972. Doi:10.1200/JCO.2009.26.3541

Table 1. Clinical and histopathological details of the patients' population

Patient	Sex	Age (y)	Location[a]	Side	Histology[b]	Seizures	KPS[c]
1	M	34	F-P	L	O II	No	100
2	M	28	F-Ins	L	OA II	No	100
3	M	33	F-T-Ins	R	O II	Yes	90
4	M	25	F-T-Ins	L	O II	Yes	90
5	F	36	F	L	A II	Yes	80
6	M	56	F-T-Ins	L	A II	Yes	90
7	F	45	F-Ins	L	O II	Yes	90
8	M	37	F-T-Ins	L	OA II	Yes	90
9	M	32	F-P	R	OA II	No	100
10	M	36	P-O	L	O II	Yes	90
11	M	30	F-T-Ins	R	A II	Yes	90
12	M	43	T	L	O II	Yes	90
13	F	38	F-T-Ins	R	A II	Yes	90
14	F	29	F	L	O II	No	90
15	M	30	F	L	OAII	Yes	90
16	M	31	F-P	L	OII	Yes	90
17	M	26	F	R	O II	Yes	90
18	F	46	F-Ins	L	O II	No	100
19	M	27	F-T-Ins	L	OA II	Yes	90
20	M	32	F-Ins	L	A II	No	100
21	F	31	F-Ins	R	O II	No	100

Note. [a] F, frontal; T, temporal; P, parietal; O, occipital; Ins, insular.

[b] According to the World Health Organization (WHO) brain tumor classification: A II, astrocytoma; O II oligodendroglioma; OA II, mixed oligoastrocytoma.

[c] KPS: Karnofsky Performance Status scale

Table 2. DTI maps histogram values (p, MD, FA) among non-progressive patients at each chemotherapy time point

	Baseline p maps (x10^{-3} mm^2/sec) (n=20)	After 3 cycles (x10^{-3} mm^2/sec) (n=15)	*p-value*	After 6 cycles (x10^{-3} mm^2/sec) (n=20)	*p-value*	Baseline MD maps (x10^{-3} mm^2/sec) (n=20)	After 3 cycles (x10^{-3} mm^2/sec) (n=15)	*p-value*	After 6 cycles (x10^{-3} mm^2/sec) (n=20)	*p-value*
mean	2.12±0.24	2.10±0.23	0.691	2.09±0.25	0.198	1.25±0.15	1.23±0.13	0.629	1.22±0.15	0.1
25th percentile	1.78±0.20	1.73±0.20	0.036*	1.65±0.22	<.0005**	1.06±0.14	1.02±0.12	0.027*	0.98±0.14	<.0005**
median (50th percentile)	2.09±0.27	2.03±0.25	0.173	1.97±0.29	0.002**	1.23±0.16	1.19±0.14	0.125	1.15±0.16	0.001**
75th percentile	2.42±0.31	2.38±0.29	0.570	2.36±0.33	0.108	1.41±0.18	1.38±0.17	0.532	1.37±0.18	0.076
interquartile range (IQR)	0.64±0.16	0.65±0.15	0.233	0.71±0.16	0.005**	0.34±0.07	0.36±0.08	0.099	0.39±0.08	0.003**
skewness	0.65±0.37	1.23±0.73	0.001**	1.43±0.57	<.0005**	0.63±0.48	1.28±0.75	0.001**	1.42±0.64	<.0005**
kurtosis	1.75±1.17	3.87±3.65	0.005**	3.76±2.60	0.001**	1.90±1.36	3.98±3.83	0.005**	3.68±2.68	0.003**

Table 2. (continue)

	Baseline FA maps (n=20)	After 3 cycles (n=15)	*p-value*	After 6 cycles (n=20)	*p-value*
mean	0.16±0.03	0.17±0.04	0.02*	0.18±0.03	<.0005**
25th percentile	0.10±0.02	0.10±0.02	0.691	0.11±0.02	0.012*
median (50th percentile)	0.14±0.03	0.15±0.03	0.551	0.15±0.03	0.004**

75th percentile	0.20±0.04	0.21±0.05	0.023*	0.22±0.05	<.0005**
interquartile range (IQR)	0.10±0.02	0.11±0.03	0.003**	0.12±0.03	<.0005**
skewness	1.60±0.50	1.57±0.57	0.427	1.50±0.56	0.391
kurtosis	5.27±3.56	4.00±2.87	0.006**	3.37±2.68	0.001**

Note: Data are interpatient means ± standard deviations. P values refer to comparisons between pre- and post-treatment measurements in non-progressive patients.

Table 3. Diagnostic performance of the best DTI histogram parameters for early identification of patients with a significant volumetric response following 6 cycles of TMZ.

Parameter	Largest Area Under the ROC Curve	*p-value*	Sensitivity (%)	Specificity (%)	Cutoff
Percentage change of 25th percentile on p maps following 3 cycles of TMZ	0.889 (0.623-0.990)	<.0001**	66.7	100	-6.47%
Percentage change of 25th percentile on MD maps following 3 cycles of TMZ	0.806 (0.525-0.959)	.019*	66.7	88.9	-6.34%
Percentage change of 75th percentile on FA maps following 3 cycles of TMZ	0.796 (0.515-0.955)	.020*	66.7	88.9	+6.59%
Percentage change of FLAIR tumor volume following 3 cycles of TMZ	0.778 (0.495-0.946)	.027*	100	55.6	-8.61%
Percentage change of FLAIR RANO product following 3 cycles of TMZ	0.800 (0.519-0.957)	.022*	80	80	-10.26%

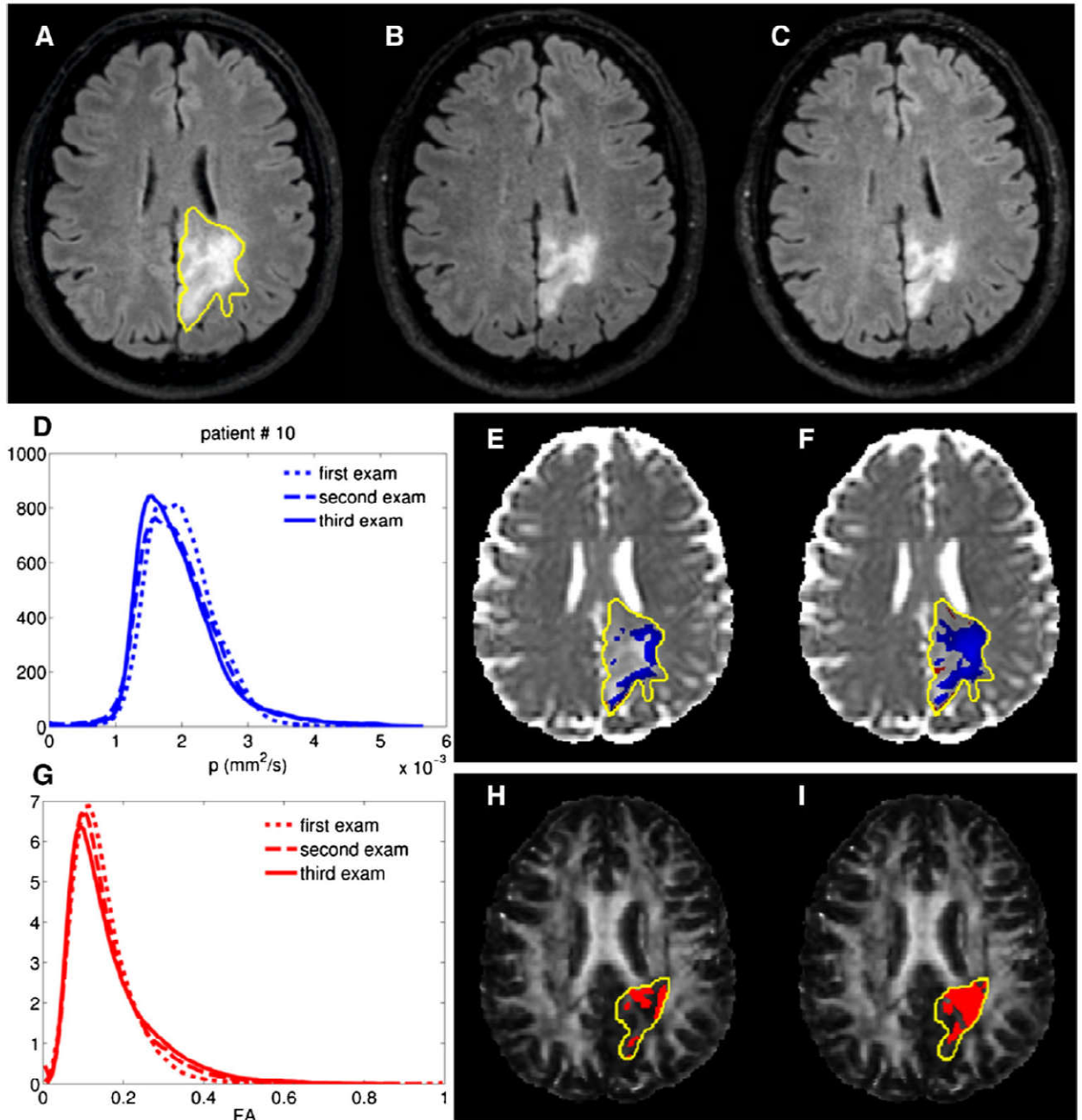Note: Number in parentheses are 95% confidence intervals.

Figure 1. Images in a 36-year-man with a recurrent low grade oligodendroglioma. (A) Pretreatment axial FLAIR image shows a left parietal hyperintense lesion, with superimposed yellow DTI *p* map ROI (E) at baseline. The area of *p* abnormality extends beyond the FLAIR hyperintensity. (B) After 3 cycles of TMZ, axial FLAIR image shows a SD, but patient had a significant clinical improvement (>50 reduction of seizures frequency). (C) Only after 6 cycles of

TMZ a mR is appreciable on FLAIR image. (D) Histograms on DTI p maps after 3 and 6 cycles reveal a continuing shift of the histogram to the left and an increase in skewness, the DTI "signature" of chemotherapy response. On fDMs after 3 (E) and 6 (F) cycles, blue voxels indicate regions with a significant decrease in pure isotropy p at each time point compared with pretreatment. Blue voxels are mainly located along the tumor borders, are already detectable after 3 cycles and become more conspicuous over time. (G) Histograms on FA maps after 3 and 6 cycles visually reveal a slight reduction of kurtosis. (H) fDMs map after 3 cycles of TMZ reveals a moderate increase of FA inside the tumor ROI (yellow line): red voxels indicate regions with a significant rise of FA values at each time point compared with pretreatment. (I) fDM analysis after 6 cycles of TMZ reveals a more conspicuos increase of FA in the whole tumor mass.
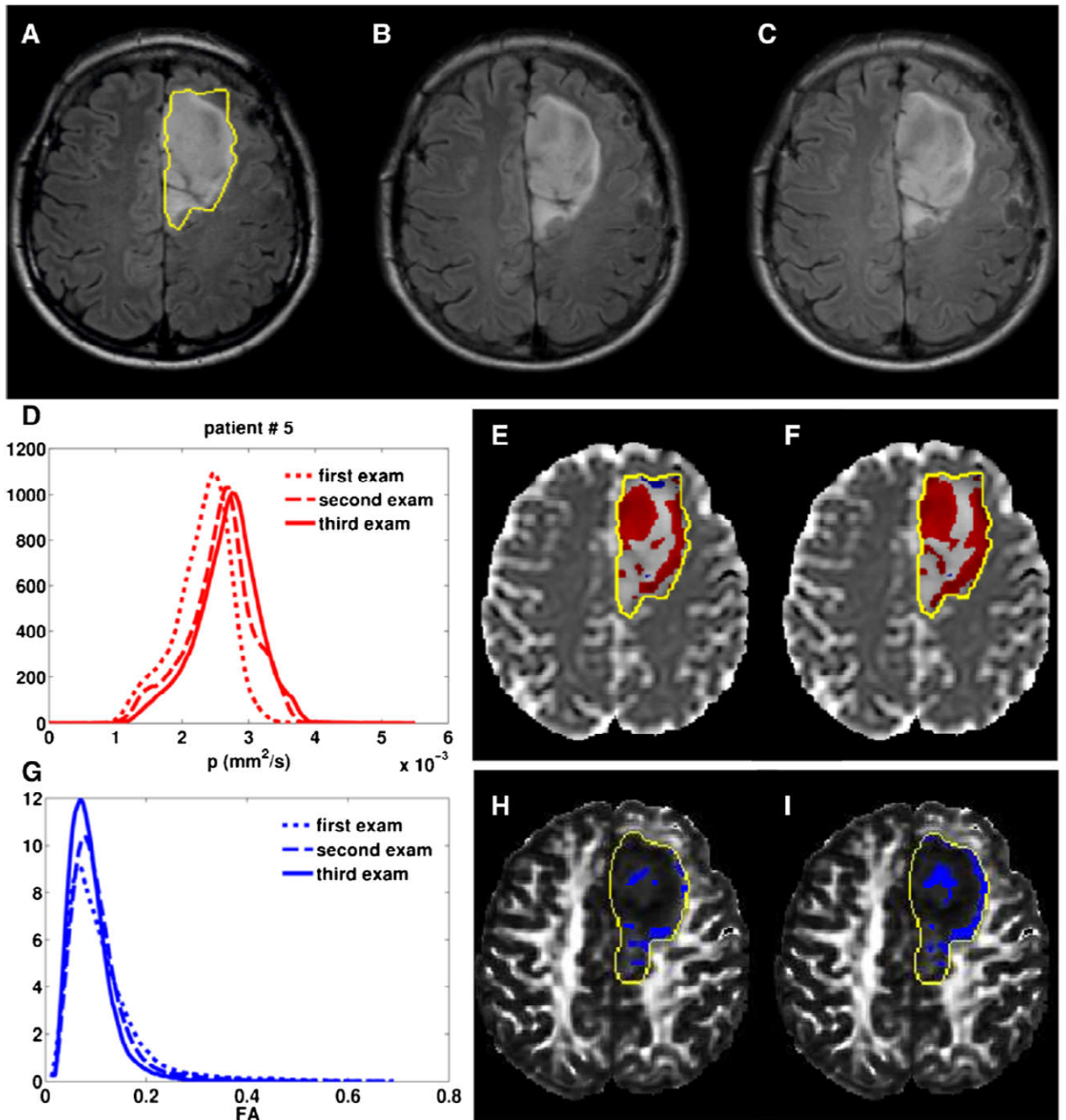
Figure 2. Images in a 36-year-woman with a recurrent low grade astrocytoma. (A)
Pretreatment axial FLAIR image shows a left frontal hyperintense lesion, with superimposed yellow
DTI p map ROI (E) at baseline. Also in this case, the area of p abnormality extends beyond the
FLAIR hyperintensity. (B) After 3 cycles of TMZ, axial FLAIR image shows a PD. (C) After 6
cycles of TMZ, axial FLAIR image confirms the progression. (D) Histograms on DTI p maps after
3 and 6 cycles reveal a continuing shift of the histogram to the right and a reduction of skewness,
the opposite pattern with respect to Figure 1. On fDMs images after 3 (E) and 6 (F) cycles, red

voxels indicate regions with a significant rise in isotropy values at each time point compared with

pretreatment; these voxels are located both along the tumor borders and inside the tumor mass,

becoming more consistent over time. (G) Histograms on FA maps after 3 and 6 cycles visually

reveal an increase of kurtosis. (H) fDM analysis after 3 cycles of TMZ reveals a moderate reduction

of FA (blue voxels) inside the tumor ROI on the FA map. (I) fDM analysis after 6 cycles of TMZ

reveals a more conspicuous reduction of FA (blue voxels) both along the tumor borders and inside
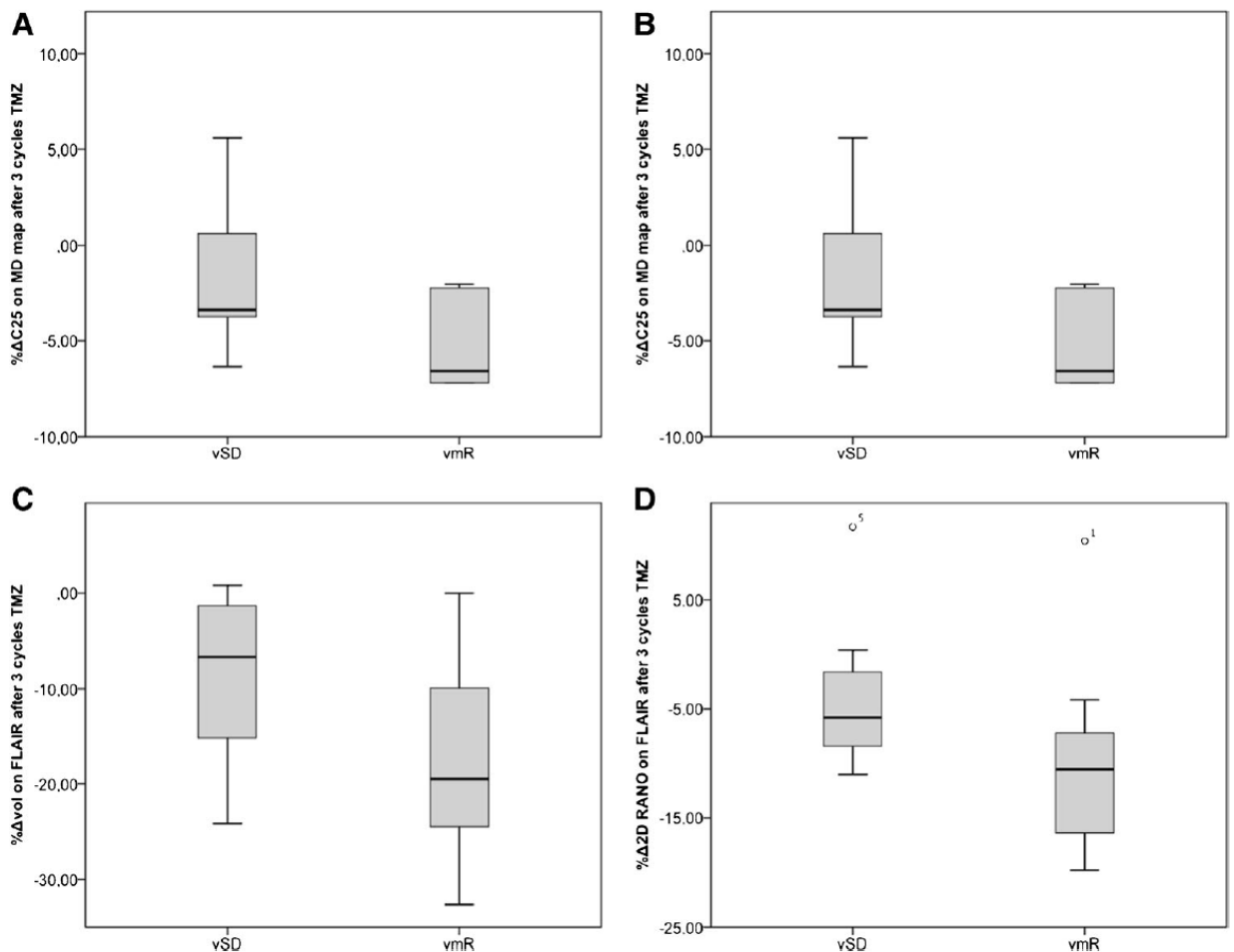
the whole tumor mass.

Figure 3. Box plots compare early percentage change of 25th percentile values (%ΔC25) on

(a) *p* map and (b) MD map and early percentage change of (c) tumor volume and (d) tumor area

according to RANO criteria on FLAIR images between stable patients after 6 cycles (vSD) and

patients with a volumetric response (vmR). Medians (line through boxes) are lower in responders

both on *p* and MD maps. Note the considerable overlap between the two groups on FLAIR images.

○ = outliers.

Electronic Supplementary Material

Details of MR Imaging Acquisitions

MR imaging was performed on a Philips Intera 3.0T system (Best, The Netherlands). Diffusion Tensor Imaging (DTI) data were obtained by using a single-shot echo planar sequence with parallel imaging (SENSE factor, 2.5). Diffusion gradients were applied along 32 axes, using a b-value of 0 and 1000 s/mm^2. The detailed imaging parameters for DTI were: repetition time msec/echo time msec (TR/TE) 8986/80; field of view (FOV) 24 cm; data matrix 96×96, interpolated in-plane to 256×256; section thickness, 2.5 mm; number of sections, 56; acquisition time, 5 minutes 23 seconds. The sequence was acquired twice and the data were averaged off-line to increase signal-to-noise ratio.

Conventional MR sequences were acquired for morphological characterization of the lesions and volumetric assessment. The MR imaging protocol included: a) axial T2-weighted turbo-spin-echo (TSE) images (TR/TE 3000/85 ms; flip angle 90°; FOV, 230 mm; 22 slices; section thickness, 5/1 mm gap; matrix, 512×512; SENSE factor, 1.5, acquisition time 3 minutes 42 seconds); b) axial T1-weighted inversion-recovery (IR) images (TR/TE/TI 2000/10/800 ms; FOV, 230 mm; 22 slices; section thickness, 5/1 mm gap; matrix, 400×512; SENSE factor, 1.7, acquisition time 4 minutes); c) axial three-dimensional fluid-attenuated inversion-recovery (3D-FLAIR) images for tumour volumetry (TR/TE/TI 10000/110/2750 ms; flip angle 90°; FOV, 230 mm; 120 slices; section thickness, 1.5/0 mm gap; matrix, 224×256; SENSE factor, 2, acquisition time 8 minutes 20 seconds) and d) post-gadolinium three-dimensional T1-weighted fast-field-echo (FFE) imaging (TR/TE 8/4 ms; flip angle 90°; image resolution equal to DTI, section thickness, 2.5 mm; no gap; 56 slices; acquisition time 1 minute 42 seconds).

All the serial MR studies were positioned by the same operator (A.I., with 20 years of experience) in order to maximize the same scan plane and angulation (anterior-posterior commissure).

Details of MR assessment of response

Response evaluation on MRI was performed *in consensus* by two board-certified neuroradiologists (A.C. and A.F.) and was based on measurement of both tumour area according to RANO criteria [13] and volume. Tumour area was considered as the product of maximum perpendicular diameters of the lesion on FLAIR images, and response was categorized as partial (PR, reduction of tumour size greater than 50% with respect to the baseline scan), minor response (mR, reduction between 25% and 50%), or progressive disease (PD, >25% increase of tumour size). A change in size between mR and PD was classified as stable disease (SD).

Tumour volume was calculated on 3D-FLAIR images using iPlan Cranial 3.0 software (Brainlab, Feldkirchen, Germany). Residual tumour margins were manually segmented on sequential axial FLAIR images by a neuroradiologist and verified in the coronal and sagittal reconstruction planes, taking advantage of the volumetric acquisition to exclude artefacts and partial volume effects. A wise inspection of further MRI sequences allowed to have a more comprehensive and robust understanding of the extension of the resection cavity. The sum of tumour segmentations of a FLAIR acquisition was automatically multiplied by slice thickness to obtain the estimated volume in cm^3, by using iPlan software. This method has been demonstrated to be reproducible and accurate to identify residual tumour on FLAIR images both in early and late postoperative MRI [29].

Response cutoffs for volumetric measurements were derived from previous correlations of bi-dimensional measures with volume [14,30]: a reduction of tumour volume greater than 65% with respect to the baseline scan was considered a volumetric partial response (vPR), while an increase of tumour volume greater than 40% with respect to the baseline scan was considered a volumetric progression (vPD). A volumetric minor response (vmR) was defined as a reduction between 32.5% and 65% of tumour volume with respect to the baseline scan while a change in size between vmR and vPD was classified as stable disease (vSD).

Details of MR-DTI data processing and analyses

DTI data were analyzed using DTI Studio v2.4.01 software (H. Jiang, S. Mori, Johns Hopkins University, Baltimore). A diffusion tensor was fitted to each voxel to obtain eigenvalues (λ_1, λ_2, λ_3), used to calculate fractional anisotropy (FA) and Trace maps. Mean diffusivity (MD) and tensor decomposition-derived pure isotropic (p) and pure anisotropic (q) maps were calculated using MATLAB 7.10.0 (The MathWorks, Natick, Massachusetts, 2010) [18].

On each map at baseline, pathological areas were analyzed using a customized automatic volumetric region-of-interest (ROI) detection tool, i.e. a CAD (Computer-Aided Detection) system for glioma recognition and segmentation, based on 3D Texture Analysis [31].

The CAD system gave automatically detected tumour regions-of-interest (ROIs). Tumour boundaries on each patient and each map were visually inspected and manually refined by a neuroradiologist (A.C.) in order to avoid false positives.

The DTI studies acquired after three and six cycles of chemotherapy were then aligned to baseline pretreatment scans. As the registration procedure was intra-subject, and studies were acquired by the same MRI scanner, a 6-dof (rigid-body) registration algorithm was used because this is the standard for serial brain on the same subject (in contrast to the nonlinear spatial transformation models, which are more suitable for intersubject registrations). In order to verify this assumption, we used SPM (Statistical Parametric Mapping, http://www.fil.ion.ucl.ac.uk/spm/) to perform both 6-parameter and 12-parameter coregistrations. We compared the 12-parameter coregistration matrices with the 6-parameter ones and verified that they were not statistically different (two-tailed Wilcoxon signed-rank test at 95% confidence level).

Moreover, the presence of an evolving tumour lesion might influence and *de facto* make incorrect any linear coregistration procedure. With the purpose of checking this hypothesis, after coregistering the patients' studies, we calculated the Mean Absolute Error (MAE) between baselines and the latest scans, limiting the calculation to the healthy hemisphere. The same procedure was applied to a set of ten control patients who underwent two DTI scans with a 6-month interval. In the latter case we arbitrarily chose one of the brain hemispheres for MAE calculation.

The two MAE distributions were compared by the Mann Whitney U test and were found statistically equivalent (at 95% confidence level), which suggests that coregistration qualities were similar for healthy and pathological images. We concluded that the presence of the tumour did not condition the coregistration procedure. Hence, we decided to simply use linear rigid coregistration, without loss of accuracy.

To quantify and analyze the heterogeneous distribution of DTI parameters in tumour regions, gray-level histograms and their main parameters (mean, median, 25th and 75th percentiles, interquartile range, skewness and kurtosis) were calculated for tumour ROIs at baseline, and compared to those from homologous contralateral regions. By using colour overlays it was also possible to visualize the distribution of histogram values in the tumour ROIs for each DTI map: an example of p map is shown in Figure S1. Blue areas indicate all the tumour voxels with DTI values below the 25th percentile, red areas indicate all the voxels with values higher than the 75th percentile and light blue areas indicate all the voxels with values between the 25th and 75th. Histogram parameters were also calculated at follow-up using the same baseline ROI to assess time evolution.

To evaluate the reliability of the automatic system, the same parameters were assessed in the tumour ROIs both before and after the manual refining, and agreement between the histogram parameters obtained for automatic and manually edited ROIs was then checked. Intraclass correlation coefficients with 95% confidence intervals were used to assess variability with respect to the parameters obtained by the completely automated procedure. Table E3 (online) summarizes the intraclass correlation coefficients (ICCs) between early measurements of DTI parameters obtained using automatic and manually refined ROIs: the high ICC values assure the equivalence of the two ROI sets for DTI parameter calculation. The excellent agreement between automatic and semi-automated procedures is an added value to implement the proposed techniques in a clinical setting.

The average execution time for the automatic procedure was about one hour per patient and map; manual refinement increased execution time by about ten minutes.

Functional Diffusion Map (fDM) analysis was performed according to the method described in [27,32] using an in-house software developed in Matlab. Each ROI on baseline map was overlaid to the respective post-treatment map, in order to compare the same brain regions and to localize therapy-induced modifications. A comparison between pre and post-therapy DTI parameters with a voxel-by-voxel approach was carried out, returning a plot (see Supplementary Figure S2 and S3) and a coloured map (Figure 1 and 2) for each patient: the plot showed data for the entire tumour volume, with the pretreatment p, q, MD and FA values on the x-axis and post-treatment respective values on the y-axis (see Supplementary Figure S2 and S3). The central green line represents equality, and the flanking blue and red lines represent the 95% confidence interval for changes in DTI maps values in the uninvolved contralateral hemisphere at baseline, including white and gray matter, in order to evaluate significant variations not due to physiological modifications between scans or to the signal noise: these thresholds for DTI values indicated that changes can be attributed with 95% probability to an underlying biologic process. Voxels in the pre-treatment DTI maps were displayed with a colour overlay of the fDMs according to the same convention as for the plot: thus, red voxels indicate regions within the tumour with a significant rise in DTI values at each time point compared with pretreatment map and blue voxels indicate areas of significant decrease in DTI values.

Furthermore, in order to assess the significance of fDM results in the pathological tissue, they were compared with the median percentage of changed voxels for p, MD and FA in the homologous contralateral regions. The percentages of blue/red voxels calculated in the contralateral regions were found to be about an order of magnitude smaller than in the pathological tissue: statistical tests showed significant differences in the distribution of the percentage values of blue voxels in p (P=0.00008), blue voxels in MD (P=0.00008), and red voxels in FA (P=.01), for the tumour region and the contralateral normal tissue both in the patients with SD according to RANO criteria and in the patient with PD. These quantitative considerations were confirmed by an evaluation of voxel-by-voxel changes of diffusion parameters on whole brain tissue between two different DTI scans

obtained from a normal subject, acquired within an interval of time consistent with the duration of the study. fDM analysis was performed in six representative ROIs containing a range of DTI values from normal gray and white matter respectively chosen in the anterior frontal regions, precentral gyrus, insula, superior parietal lobule, temporal lobe and in the white matter of the centrum semiovale. The 95% confidence intervals for changes in DTI map values were found to be well in the range of those chosen on the basis of the analysis of patient contralateral regions.

A final assessment of our results included a verification of the long-term stability of the DTI acquisitions, with a comparison of the histogram results in these ROIs in the control subject and the calculation of the percentage of difference between gray-level medians. In each DTI map of the two different datasets (hereafter named I_1 and I_2), the gray-level histograms of the voxels within each ROI were very well overlaid, as indicated by a preliminary visual inspection. For each map and each ROI, the percent difference between gray-level medians (med) was calculated as $\%\Delta med = 100 \cdot (med(I_2) - med(I_1)) / med(I_1)$: isotropic maps ($p$, MD) gave $\%\Delta med \approx 1\%$, while anisotropic ones (FA, q) gave $\%\Delta med < 3\%$. The percentage of changes of histogram parameters in patients' pathological tissue is far beyond these small differences found in the control subject. Finally, the correlation coefficients between I_1 and I_2 voxels (in each ROI) were calculated and were higher than 0.9, confirming the good image acquisition stability over time.
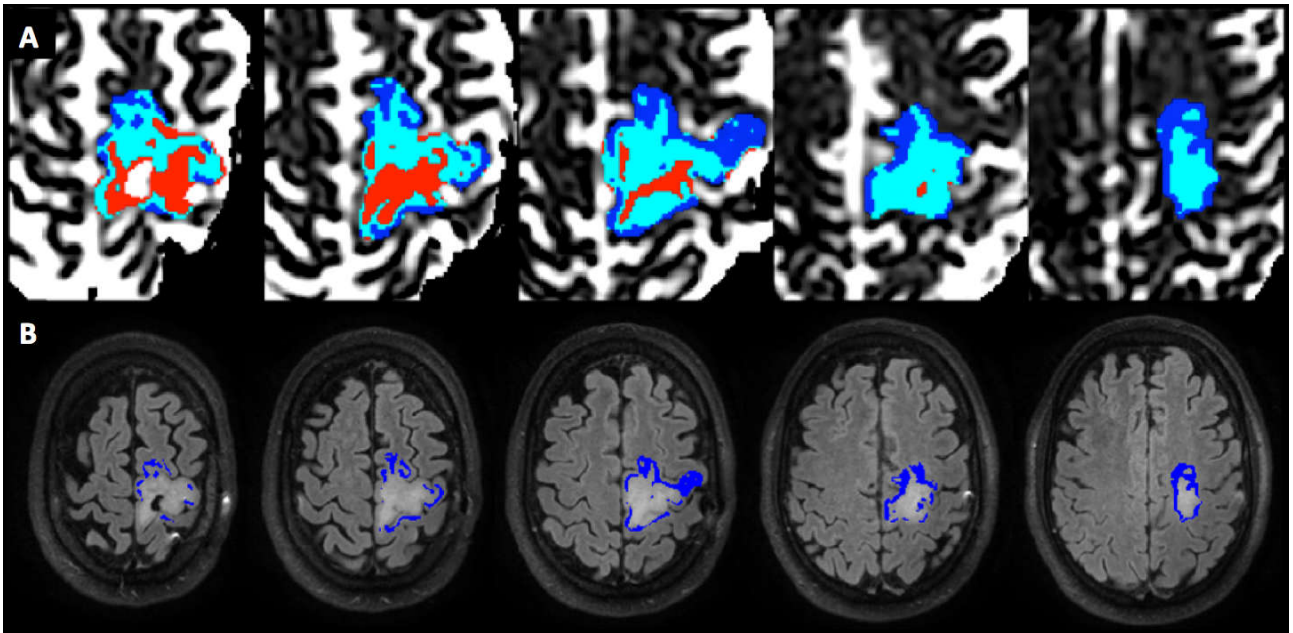
Figure S1. Visualization of the distribution of histogram values within the tumour ROIs on p map in a case of oligodendroglioma. (A) Blue areas indicate all the tumour voxels with values of p below the 25th percentile, red areas indicate all the voxels with values higher than the 75th percentile and light blue areas indicate all the voxels with values between the 25th and 75th. Visual inspection indicates that the median p values are located within the centre of the tumour, whereas the lower 25th percentile of p are typically located at the edge of the tumour. (B) Interestingly, the blue areas containing the voxels with values of p below the 25th percentile extends beyond the edge of the FLAIR alteration.
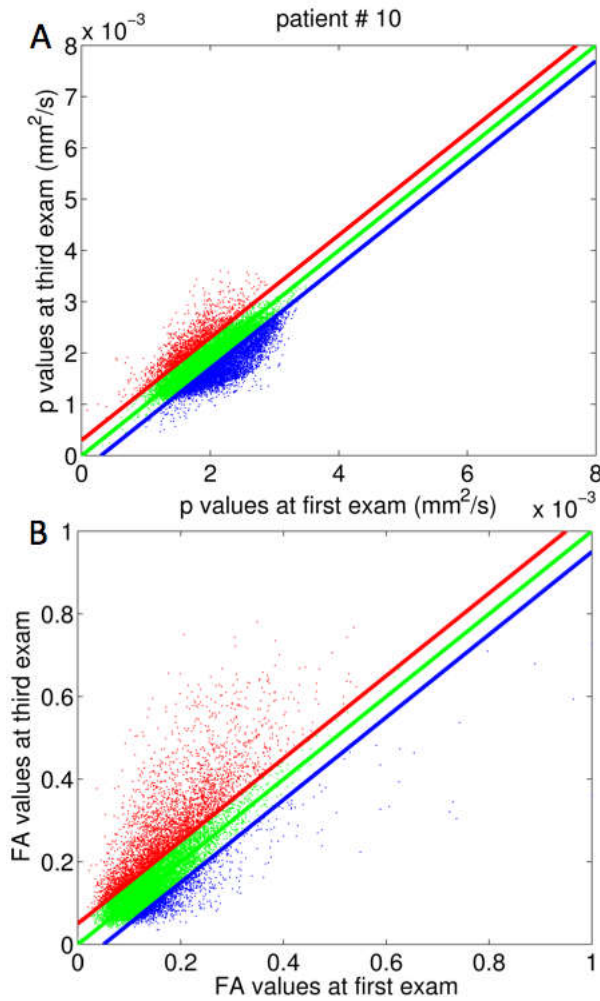
Figure S2. Scatter plot from fDMs analysis display data for the entire tumour volume in the same patient with a positive response to treatment showed in Figure 1. Each point represent one voxel in tumour tissue. Pretreatment DTI (A) pure isotropy p values and (B) FA values are reported on the x-axis and post-treatment values on the y-axis. (A) The blue dots indicate voxels with decreased values of p over time, whereas the red and green dots indicate regions of increased and unchanged p, respectively. There is a prevalence of blue voxels, indicating a reduction of isotropy over time after treatment. (B) The red dots indicate voxels with increased FA values over time, whereas the blue and green dots indicate regions of decreased and unchanged FA, respectively. There is a net increase of FA values over time after treatment.
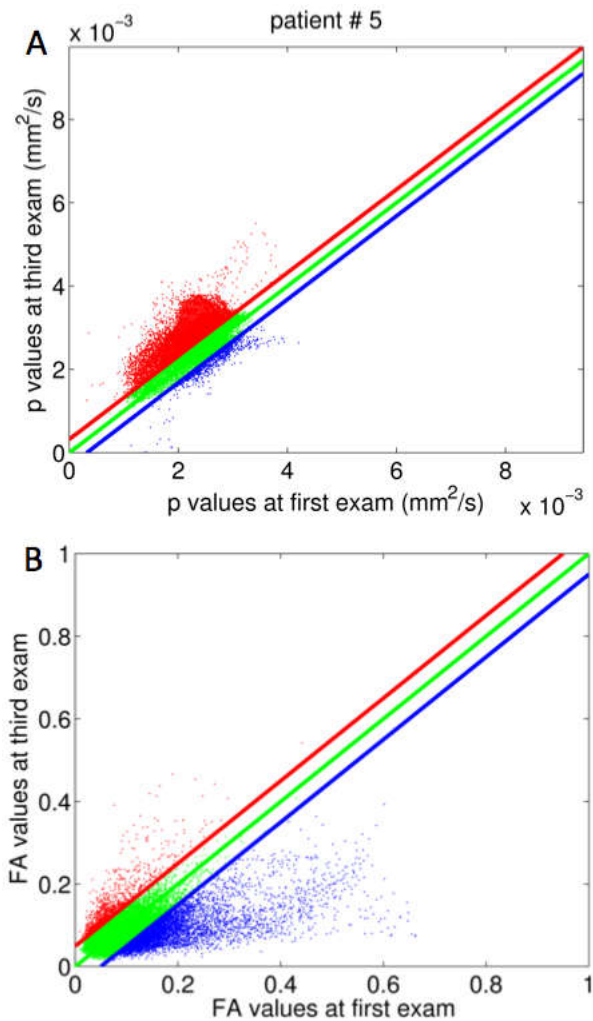
Figure S3. Scatter plot from fDMs analysis display data for the entire tumour volume in the same patient with a negative response to treatment showed in Figure 2. Each point represent one voxel in tumour tissue. Pretreatment DTI (A) pure isotropy *p* values and (B) FA values are reported on the x-axis and post-treatment values on the y-axis. (A) The red dots indicate voxels with increased values of *p* over time, whereas the blue and green dots indicate regions of increased and unchanged *p*, respectively. There is an evident prevalence of red voxels, indicating an increase of isotropy over time and a negative response to treatment. (B) The blue dots indicate voxels with decreased FA values over time, whereas the red and green dots indicate regions of increased and unchanged FA, respectively. There is a net decrease of FA values, suggesting a progressive alteration of the tumour structure over time after treatment.

Table E1 (online). DTI maps histogram values at baseline

n=21	tumour MD maps (x10^{-3} mm^2/sec)	contralateral MD maps (x10^{-3} mm^2/sec)	*p-value*	tumour FA maps	contralateral FA maps	*p-value*
mean	1.25±0.14	0.97±0.15	**<0.001****	0.15±0.03	0.25±0.02	**<0.001****
25th percentile	1.07±0.13	0.73±0.04	**<0.001****	0.10±0.02	0.11±0.02	0.079
median (50th percentile)	1.24±0.16	0.82±0.05	**<0.001****	0.14±0.03	0.21±0.04	**<0.001****
75th percentile	1.41±0.17	1.08±0.35	**0.002****	0.19±0.04	0.36±0.04	**<0.001****
interquartile range (IQR)	0.34±0.07	0.35±0.34	0.099	0.10±0.02	0.25±0.04	**<0.001****
skewness	0.57±0.53	2.44±0.79	**<0.001****	1.64±0.52	0.71±0.29	**<0.001****
kurtosis	1.84±1.36	8.83±6.14	**<0.001****	5.42±3.55	0.09±0.67	**<0.001****

Note: Data are interpatient means ± standard deviations.

Table E1. (continue)

n=21	tumour p maps (x10⁻³ mm²/sec)	contralateral p maps (x10⁻³ mm²/sec)	p-value	tumour q maps (x10⁻³ mm²/sec)	contralateral q maps (x10⁻³ mm²/sec)	p-value
mean	2.13±0.24	1.68±0.25	**<0.001****	0.25±0.04	0.30±0.05	**0.004****
25th percentile	1.79±0.21	1.26±0.06	**<0.001****	0.18±0.04	0.17±0.04	0.079
median (50th percentile)	2.11±0.27	1.41±0.07	**<0.001****	0.24±0.04	0.26±0.05	0.305
75th percentile	2.42±0.30	1.89±0.65	**0.002****	0.31±0.05	0.39±0.07	**<0.001****
interquartile range (IQR)	0.63±0.15	0.63±0.65	0.073	0.13±0.02	0.23±0.05	**<0.001****
skewness	0.59±0.45	2.42±0.76	**<0.001****	0.88±0.43	1.03±0.40	0.181
kurtosis	1.68±1.19	8.61±5.92	**<0.001****	1.85±2.65	1.16±1.21	0.357

Note: Data are interpatient means ± standard deviations.

Table E2 (online). Correlation between percentage changes in DTI histogram parameters after 3 cycles and final percentage changes of tumour volume following 6 cycles of TMZ.

N=16	Percentage change of tumour volume after 6 cycle					
Percentage change after 3 cycles	ρ	*p-value*	ρ	*p-value*	ρ	*p-value*
mean	**0.744**	**(0.001**)**	**0.521**	**(0.039*)**	**-0.576**	**(0.019*)**
25th percentile	**0.765**	**(0.001**)**	**0.670**	**(0.005**)**	-0.229	(0.393)
median (50th percentile)	**0.692**	**(0.003**)**	**0.559**	**(0.024*)**	**-0.653**	**(0.006**)**
75th percentile	**0.665**	**(0.005**)**	**0.571**	**(0.021*)**	**-0.588**	**(0.017*)**
interquartile range (IQR)	0.209	(0.438)	0.197	(0.464)	**-0.582**	**(0.018*)**
skewness	-0.491	(0.053)	**-0.588**	**(0.017*)**	**0.621**	**(0.010*)**
kurtosis	-0.294	(0.269)	**-0.618**	**(0.011*)**	**0.791**	**(<0.0005**)**
	p map		**MD map**		**FA map**	

Note: Data are Spearman rank correlation coefficients (ρ), with p-values in parentheses.

Table E3 (online). Intraclass correlation coefficients (ICC) for measurements of the best early DTI

histogram parameters with semi-automatic (saROIs) and automatic (aROIs) methods.

Parameter	ICC	*p-value*
Percentage change of 25th percentile on p maps following 3 cycles of TMZ	0.985 (0.956-0.995)	**<0.0001****
Percentage change of 25th percentile on MD maps following 3 cycles of TMZ	0.965 (0.899-0.988)	**<0.0001****
Percentage change of 75th percentile on FA maps following 3 cycles of TMZ	0.941 (0.816-0.980)	**<0.0001****

Note: Number in parentheses are 95% confidence interval.